DYNAMICS OF JUPITER'S ATMOSPHERE

A.P. INGERSOLL AND A.R. VASAVADA
California Institute of Technology
Division of Geological and Planetary Sciences
Pasadena, CA 91125

AND

THE GALILEO IMAGING TEAM
Jet Propulsion Laboratory
Pasadena, CA 91109

Abstract. Results from the Galileo probe and orbiter are compared with Voyager and ground-based results. The probe made measurements to the 20-bar level, well below the nominal cloud base at 5 bars and well below the level where sunlight is absorbed. The winds increased with depth within the clouds and then remained constant below cloud base. This rules out most "thin weather layer" models of Jovian meteorology. Water, H_2S, and NH_3 were depleted relative to "solar" abundances at the nominal cloud base but increased with depth below 10 bars. Apparently the probe entered a dry downdraft that penetrated to 20 bars. Consistent with this result, the orbiter found water varying by factors of 100 from place to place, with the lowest values at the sites that resemble the one where the probe went in. The orbiter also revealed that these sites are regions of horizontal convergence of the cloud top winds, which is consistent with the downdraft hypothesis.

1. Introduction

The Voyager era spanned a decade from the two Jupiter encounters (Smith et al. 1979a,b) to the Neptune encounter in 1989. During that time we measured wind patterns at 100 km per pixel resolution (Earth-based resolution is 3000 km per pixel), temperatures at altitudes ranging from 1 bar to 1 mbar, and composition above the 1-bar level (Ingersoll 1990). Over most of the planet the cloud tops are at 0.5 to 1.0 bar, and Voyager's remote sensing instruments cannot see below this level.

The Galileo probe promised to measure winds, temperatures, composition, and radiative fluxes to 10 or 20 bars, which is well below cloud base assuming a "solar" mixture of elements. The Galileo orbiter promised to image the planet at 25 km per pixel, and possibly detect the primary convective elements analogous to terrestrial thunderstorms.

Figure 1 (see color plates) shows a Voyager image of Jupiter on the right and a simultaneous Earth-based infrared image on the left (Terrile and Beebe 1979). The Great Red Spot (GRS), a giant storm that has been in existence for at least 100 years, is visible in both images. The colors in the visible image reflect the different chemical compositions of the cloud particles. The colors in the infrared image reflect the different depths from which the radiation is emerging. The infrared data were taken with a filter that is sensitive only to light in the range from 4 to 5 microns, where Jupiter's atmospheric gases are relatively transparent. At the places where the clouds are thin or transparent, infrared emission from warmer, deeper layers escapes to space. At the places where the clouds are thick and opaque, only infrared radiation from the colder cloud tops can escape. The Galileo probe entered the atmosphere in one of the transparent regions — a so-called "5-micron hotspot" in the band at 6.5° planetocentric latitude.

Figure 2 shows the zonal wind profiles for the four giant planets (Ingersoll et al. 1995). The winds are measured relative to the interior of the planet, whose speed of rotation is inferred from

J. Andersen (ed.), Highlights of Astronomy, Volume 11B, 1042–1049.

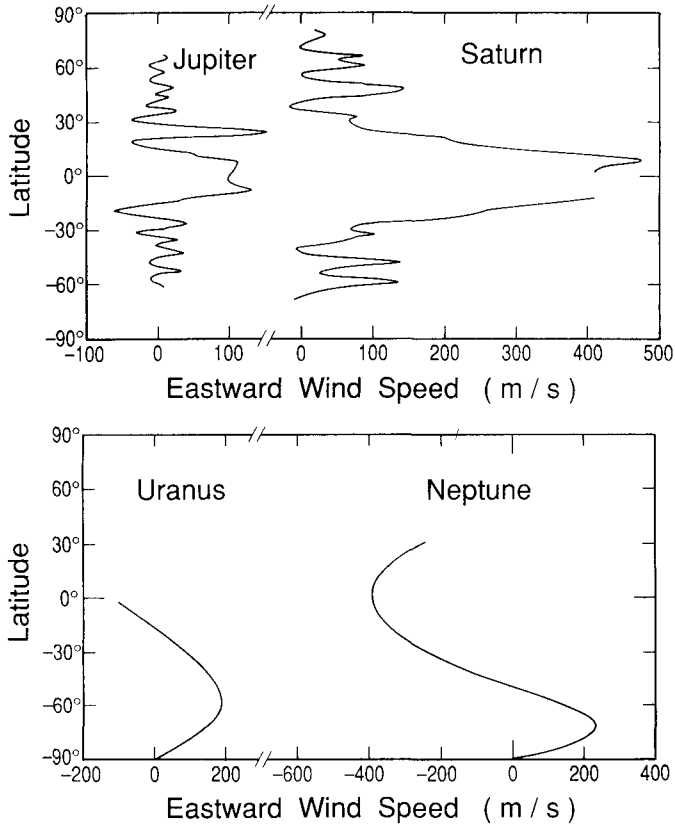

Figure 2. Zonal wind profiles for the giant planets. The ordinate is latitude and the abscissa is eastward velocity relative to the planet's interior as defined by the magnetic field and radio emissions (Fig. 26 of Ingersoll et al. 1995).

the magnetic field and associated radio emissions. Surprisingly, the winds do not decrease as one moves out in the Solar System. For instance, the winds at Neptune are 2.5 times stronger than at Jupiter, even though the power per unit area (total infrared emission or total absorbed sunlight) is 20 times less. The explanation may be that the energy sources — sunlight and internal heat — drive small-scale convection which acts as a dissipative mechanism. The turbulence level, and hence the eddy viscosity, is higher in the atmosphere of Jupiter than it is in the atmosphere of Neptune, so the large-scale winds are less at Jupiter. Neptune's zonal winds are coasting along with very little dissipation.

Figure 3 shows the infrared emission as a function of latitude. The ordinate is total power radiated (at all wavelengths) per unit area. In contrast to the 5-micron emission (Fig. 1), which is sensitive to holes in the clouds, the total power depends mainly on the temperature of the gas in the 0.3- to 0.5-bar range, which is generally above the tops of the clouds. The equivalent brightness temperatures are given at right. The bumps in the curves are associated with the banded clouds (Fig. 1) and zonal jets (Fig. 2). But overall the curves are remarkably flat. On Earth, the radiated power per unit area is markedly peaked at the equator because it is warmer there than at the poles. On the giant planets the poles and equator are at about the same temperatures, even though sunlight heats one part of the planet more than the other (on Jupiter, Saturn, and Neptune, the Sun heats the equator more than the poles; on Uranus it heats the poles more than the equator). Thus the heat transfer must be efficient enough to eliminate any horizontal temperature gradients that solar heating would produce. Whether this heat transfer takes place in the atmospheres or

https://doi.org/10.1017/S1539299600019560 Published online by Cambridge University Press

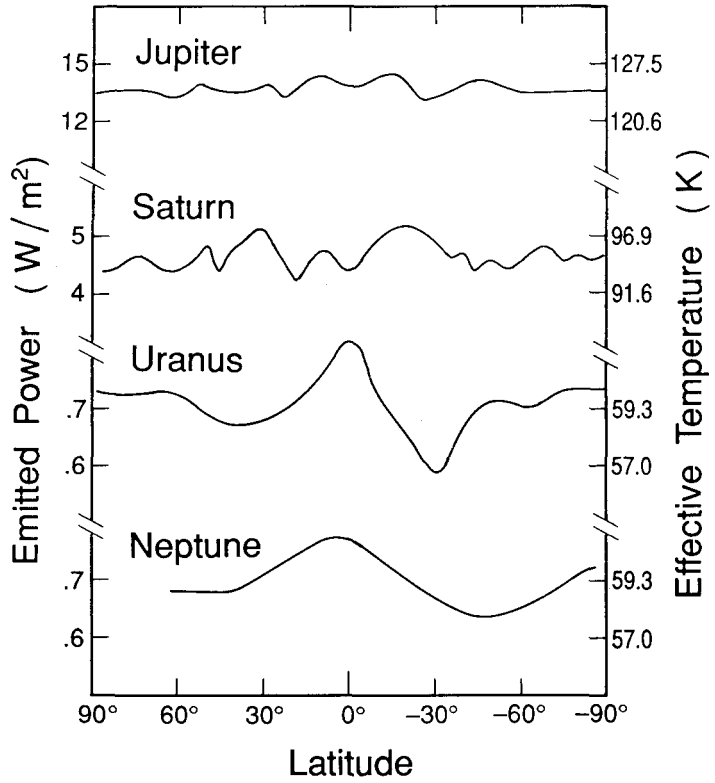

Figure 3. Emitted power and equivalent brightness temperature for the giant planets (Fig. 25 of Ingersoll et al. 1995).

in the fluid interiors of the giant planets is an interesting but unresolved question (Ingersoll and Porco 1978; Friedson and Ingersoll 1987).

The Voyager encounters and Earth-based observations were limited in two main respects. First, they did not provide information on phenomena smaller than about 100 km, which is several times larger than the atmospheric scale height and thus several times larger than the primary convective elements — the thunderstorms and cumulus clouds that play such an important role in moving heat upward in the Earth's atmosphere. Second, the remote-sensing observations did not penetrate into the clouds. The Galileo mission was designed to address these issues.

2. Galileo Probe

Figure 4 is a pre-Galileo model of the vertical structure of Jupiter's atmosphere (Atreya 1986). It is based on several assumptions; first, that the atmosphere is convective from the tops of the clouds downward. This sets the temperature profile, since temperature is known above the tops of the clouds and convection produces an "adiabatic" temperature gradient. Second, the abundances of CH_4, NH_3, H_2S, and H_2O relative to H_2 and He are computed from a "solar composition" model, in which the elements C, N, S, O, H, and He are present with the same proportions as on the Sun (both the solar and the 10^{-3} solar cases are shown for water). As temperature falls with altitude (see scale at left), each gas condenses out at a specific level, which defines cloud base for that constituent. The third assumption is that all the condensate remains in the cloud, which leads to the cloud densities shown along the bottom of the figure. However, analogy with the Earth suggests that most of the condensate falls out. Thus the figure provides only an upper bound on the expected cloud densities.

https://doi.org/10.1017/S1539299600019560 Published online by Cambridge University Press

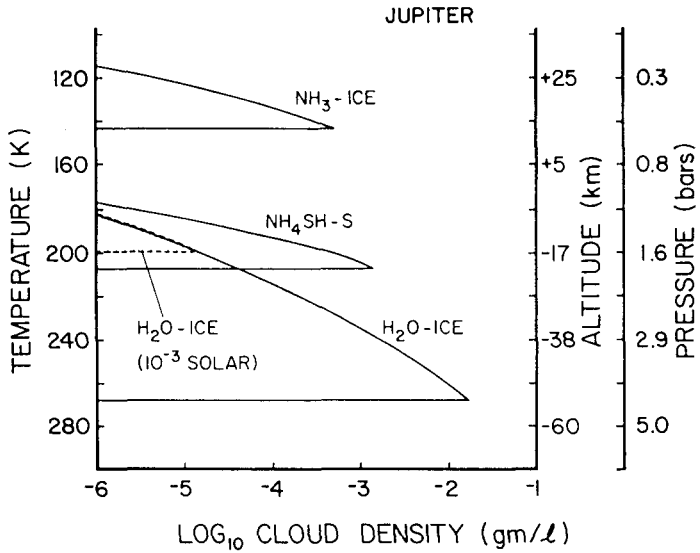

Figure 4. Model of the cloud structure at Jupiter (Fig. 3.2 of Atreya 1986). Altitudes are relative to the 1-bar pressure level.

It was thought that Jupiter's atmosphere would be chemically homogeneous and well-mixed below the base of the water cloud. For a solar composition atmosphere, cloud base is at 5 bar (Fig. 4). Increasing the water abundance moves cloud base to deeper levels, but even a 10-fold enrichment moves it down only a few bars. The expectation that the atmosphere would be chemically homogeneous was based on the observation that Jupiter has an internal heat source. That is, the total power radiated by the planet in the infrared is 1.7 times that absorbed from sunlight. The difference is stored internal heat that has been slowly escaping over the age of the Solar System. This internal heat is carried to the surface by convection currents, which stir the atmosphere. The much slower large-scale vertical motions associated with the bands and jets (Fig. 1) cannot compete with this vigorous stirring. That was the assumption before Galileo.

The 5-micron hotspots, like the one the probe entered, are thought to be downdrafts thousands of km across. Air is dried out in its ascent from the deep atmosphere, and it remains dry during descent. The lack of condensables accounts for the transparency of the clouds in the 5-micron hotspots. The surprising result from the Galileo probe is that hotspots have deep roots that extend well below cloud base. The evidence is that NH_3, H_2S, and H_2O all increase with depth in the 10- to 20-bar range. The H_2S results come from the probe's mass spectrometer experiment (Niemann et al. 1996, 1997). The value at 8 bars was much less than the "solar" value, but rose to 2.7 × solar at the deepest levels sampled. The NH_3 results come from attenuation of the probe's radio signal (Folkner and Woo 1997). The value increases from much less than solar at 4 bars to 3.3 × solar below 10 bars. Above the 10-bar level the water results come from the probe's net flux radiometer (Sromovsky et al. 1996) and from the mass spectrometer (Niemann et al. 1996). Near 10 bars the mixing ratio is 0.2 × solar, but it increases with depth and the asymptotic value has not been determined (Atreya et al. 1997; Niemann et al. 1997).

Since CH_4 does not condense on Jupiter, it is present above the clouds and can be measured from Earth. The probe verified that the abundance is 2.9 × solar (Niemann et al. 1996), which is similar to the abundance of N and S relative to solar. Models of Solar System formation generally have C, N, S, and O all enriched by about the same amount.

The water abundance is a major unanswered question. Estimates based on remote sensing range from 0.02 × solar (Bjoraker et al. 1986) to arbitrarily large values (Carlson et al. 1992). Indirect inferences from the speed of waves that followed the Shoemaker-Levy 9 impacts (Ingersoll and Kanamori 1995) yield a water abundance of 10 × solar. Condensation of water affects the

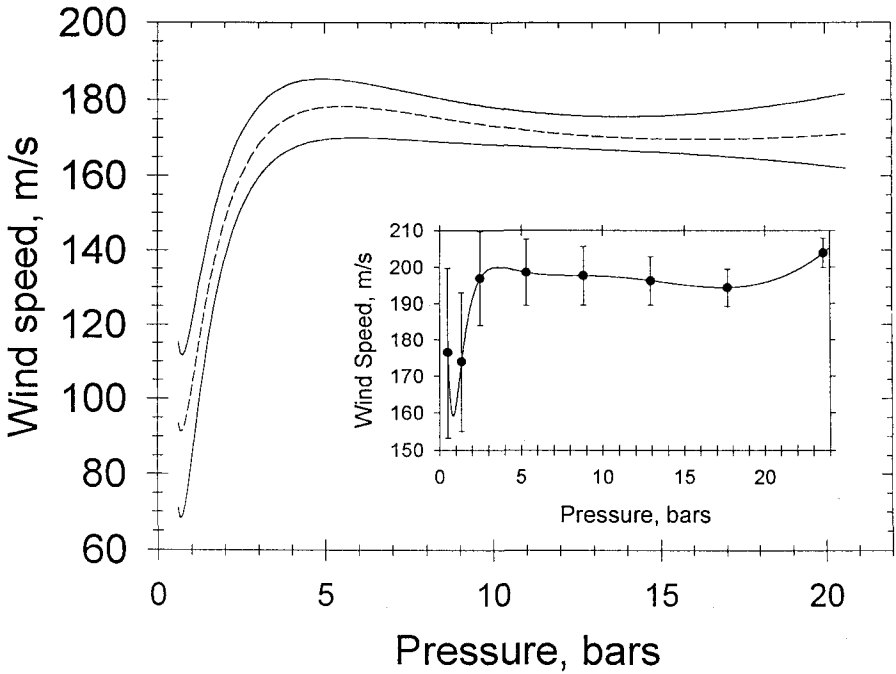

Figure 5. Eastward wind speed versus depth as inferred from the Doppler Wind Experiment on the Galileo probe (Fig. 1 of Atkinson et al. 1997). The insert is from a preliminary analysis of the data.

vertical thermal structure (atmospheric stability) and the mode of vertical heat transport, so it plays a major role in atmospheric dynamics. The dry downdraft hypothesis is the most plausible. To remain dry, a downdraft must be less dense than the surroundings if the surroundings have greater than solar abundance of water (Showman and Ingersoll 1997). Energy from other parts of the atmosphere is needed to push the low density air downward. The energy is sufficient, but the specific mechanisms have not been identified (Showman and Ingersoll 1997).

Figure 5 shows the results of the Doppler wind experiment (Atkinson et al. 1996, 1997; Folkner et al. 1997). The winds increased with depth from 100 ms^{-1} at the 0.7 bar level to 170 ms^{-1} at 4 bars, and then remained constant down to the 21 bar level where the probe data ended. The value at the upper level is consistent with cloud-tracked winds at the 6.5° latitude where the probe went in (Fig. 2), but the value at the bottom was a surprise. Most theories postulated that the winds would either decrease or remain constant with depth (Ingersoll and Cuzzi 1969; Ingersoll and Cuong 1981; Pollack et al. 1992). Only one theory predicted that the winds would increase with depth (Dowling 1995), and that was based on the controversial "wave" interpretation of the Shoemaker-Levy 9 observations (Hammel et al. 1995; Ingersoll and Kanamori 1995).

The probe results imply that the winds are "deep," since they are strong below cloud base. Latent heat release and absorption of sunlight occur within the clouds (Sromovsky et al. 1996) so it is tempting to conclude that the deep winds are driven by internal heat. That might be a premature conclusion (Atkinson et al. 1997). In a rotating fluid planet whose interior is well-mixed by convection (i.e., with an adiabatic, barotropic interior), the fluid elements are tied together in columns parallel to the rotation axis. Each column moves as a unit, so energy input at one level is felt at all other levels. In this way, convection near the surface could drive motions in the interior, or vice versa. Whatever the ultimate energy source for the winds, the fact that they are deep has important implications for the dynamics by providing a lower boundary condition for motions in the visible cloud layers (Dowling and Ingersoll 1989).

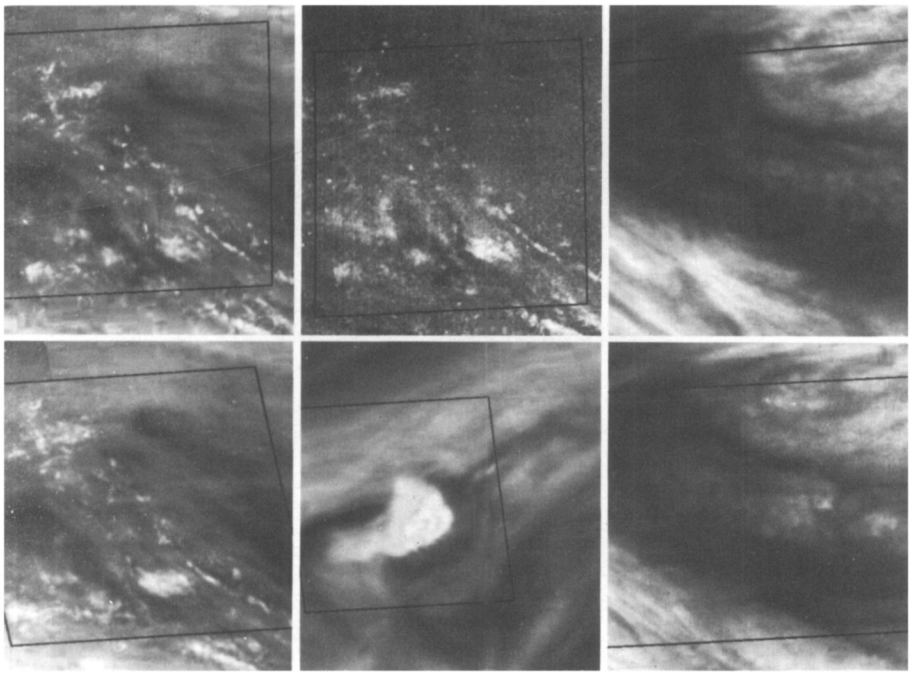

Figure 7. High-resolution views of the area around Jupiter's Great Red Spot. Panels A and B (upper left and lower left) are separated in time by 75 minutes. Panel C (top center) is taken in the strong methane band at the same time as A to show high clouds. Panel D (lower center) is a high, thick cloud to the northwest of the Great Red Spot. Panels E and F (upper right and lower right) are separated in time by 9 hours and show a region of transient wave activity (Fig. 4 of Belton et al. 1996; p-47938).

3. Galileo Orbiter

The imaging system on the orbiter regularly imaged Jupiter at 25 – 30 km resolution. The relatively high spatial resolution and the high temporal resolution (the typical time interval between images was 75 minutes) means that rapid, small-scale features could be followed over their life cycles. In addition, the sensitivity of the camera to 1-micron wavelength means that clouds at different altitudes could be followed separately in different filters. The 889-nm filter overlaps a strong methane absorption band, so only high clouds are visible in this filter. The 727-nm filter overlaps a weak methane band, so both intermediate and high clouds are visible. Clouds at all levels are visible in the 756-nm filter, which does not overlap any methane bands.

Figure 6 (see color plates) shows a false-color image of the Great Red Spot (GRS), where the 889-nm filter image is shown as blue, the 727-nm filter image is shown as green, and the 756-nm filter image is shown as red (Vasavada et al. 1997). High, thin clouds appear blue, since they have a relatively large effect in the strong methane (889-nm) filter. High, thick clouds appear white, since they scatter light in all filters. Low clouds appear red, since they are invisible in the methane (727-nm and 889-nm) filters. Intermediate clouds appear yellow (756-nm and 727-nm), and high, thin clouds overlying deep clouds appear purple (889-nm and 756-nm). From the variety of colors visible in the figure, it is clear that a variety of cloud types exist on Jupiter. The GRS is covered by a high, thin cloud. A smaller and much thicker high cloud is visible to the northwest, and numerous small-scale thick clouds are visible to the north and northeast.

Figure 7 shows some high-resolution views of the regions around the GRS (Belton et al. 1996). The smallest features are 30 km in size. Panels A and B are a time sequence of the region to the northeast of the GRS showing the rapid changes that occur over the 75-minute time interval. Panel C is the same as A but in the strong methane band (889-nm). Panel D is the bright spot to the northwest of the GRS. Panel E shows waves in the clouds. Panel F shows the same region 9 hours

later and the waves have dissipated. The small, rapidly-varying features in Panels A, B, and C are probably Jovian thunderstorms.

Figure 8 (top) (see color plates) shows a pseudo true-color view of a 5-micron hotspot (Vasavada et al. 1997). The violet filter was used for blue; the 756-nm filter was used for red, and a mixture of violet and 756-nm filter was used for green. The colors are due to the absorptions of the different cloud particles in Jupiter's atmosphere. Figure 8 (bottom) shows a false-color image using the same scheme as Fig. 6. The colors are due to the different heights of the clouds. The hotspot is a hole in the deep clouds but is overlain by high, thin haze. The area to the east contains possible thunderstorms — high, thick clouds in small clusters that change rapidly over a 75-minute interval.

Figure 9 (see color plates) shows a summary of the winds deduced from sequences of images, in the reference frame of the hotspot (Vasavada et al. 1997). Strong winds converge on the central region from the southwest, but no comparable winds seem to exit the region. The inference is that the center is a downwelling region, since the winds are observed at the tops of the clouds and horizontal convergence must be balanced by vertical divergence. With somewhat better temporal and spatial resolution, as planned for the Galileo Europa Mission, it should be possible to estimate the rate of convergence and hence the speed of the downdraft. This will help in evaluating theories of the volatile depletion measured by the probe.

The Near Infrared Mapping Spectrometer (NIMS) was able to measure the water-vapor distribution both inside and outside the 5-micron hotspots (Roos-Serote et al. 1997). They found that water vapor varies from place to place by a factor of 100, and the hotspots are the driest places. The probe hit a dry part of the planet, but Jupiter as a whole is not dry.

Figure 10 (see color plates) shows pseudo true-color (particle composition) and false color (cloud altitude) views of oval storm systems at $-22°$ to $-38°$ planetocentric latitude (Vasavada et al. 1997). The two large pale blue features are the classic white ovals that formed in 1938. The smaller blue feature to the southeast is a member of the same class but without a name or pedigree. The GRS, which is 20,000 km long, is the largest member of the class, which includes all long-lived anticyclonic ovals down to scales of 1000 km (MacLow and Ingersoll 1986). Anticyclones are high-pressure systems and rotate counterclockwise in the southern hemisphere. The blue color in the lower image suggests that the anticyclones have high clouds. The yellow feature between the ovals is a cyclone. Its color indicates that the clouds are low. The flow (not shown) passes south of the left white oval, impinges on the cyclone from the southwest, piles up in a set of high, thick clouds (white area), and then flows north of the cyclone and down the other side, exiting eastward on the south side of the right white oval. These data will help modelers trying to simulate the complex interactions between these structures and ultimately account for their long life and stability. Comparable structures in the Earth's atmosphere rarely last longer than a week or 10 days.

Figure 11 (see color plates) shows the Jovian aurora on the night side of the planet (Ingersoll et al. 1997). The sunlit part of the planet is out of the frame to the right, and covers slightly more than half the disc. The violet filter is projected as blue, the clear filter as green, and the red filter as red. In this projection the aurora appears white, while stray light from Jupiter scattered off the inside of the camera appears green. As on Earth, the Jovian aurora is generated when charged particles strike the upper atmosphere from above. The particles follow magnetic field lines, and the narrowness of the arc suggests a narrow source region for the particles. The field lines that intersect the planet at this particular latitude ($54.5° \pm 0.3°$ planetocentric) cross the equatorial plane at 13 – 14 Jovian radii from the planet center, somewhere between the orbits of Europa and Ganymede. Whether there is something special about this region is not clear.

Galileo will continue taking observations until the year 2000. In the near term, a 4-hour movie of the aurora is planned. We will search for lightning on the night side, and will image the same cloud features 2 hours later on the day side to positively identify the thunderstorms. There will be intensive mapping of water vapor to find out what kinds of dynamical features are wet and what kind are dry. Finally, we plan a series of 8-frame movies at 12- to 15-km resolution to study the most rapidly-varying phenomena — waves and convection — at the smallest spatial scales. It should be a wild ride.

Acknowledgements

It is impossible to mention all the people who contributed their talent and energy to the success of the Galileo project. Their achievement is gratefully acknowledged.

References

Atkinson, D.H. et al. (1997) *Nature*, **388**, pp. 649–650.
Atreya, S.K. (1986) *Atmospheres and Ionospheres of the Outer Planets and Their Satellites*, Springer Verlag, New York.
Atreya, S.K. et al. (1997) In: *Three Galileos: The Man, The Spacecraft, The Telescope*, J. Rahe, C. Barbieri, T. Johnson, A. Sohus (Eds.), Kluwer Academic Publishers, Dordrecht.
Belton, M.J.S. et al. (1996) *Science*, **274**, pp. 377–385.
Bjoraker, G.L. et al. (1986) *Icarus*, **66**, pp. 579–609.
Carlson, B.E. et al. (1992) *Astrophys. J.*, **388**, pp. 648–668.
Dowling, T.E. and A.P. Ingersoll (1989) *J. Atmos. Sci.*, **46**, pp. 3256–3278.
Dowling, T.E. (1995) *Icarus*, **117**, pp. 439–442.
Folkner, W.M. et al. (1997). *Science*, **275**, pp. 644–646.
Folkner, W.M. and R. Woo (1997) *J. Geophys. Res.*, in press.
Friedson, J. and A.P. Ingersoll (1987) *Icarus*, **69**, pp. 135–156.
Hammel, H.B. et al. (1995) *Science*, **267**, pp. 1288–1296.
Ingersoll, A.P. (1990) *Science*, **248**, pp. 308–315.
Ingersoll, A.P. and J.N. Cuzzi (1969) *J. Atmos. Sci.*, **26**, pp. 981–985.
Ingersoll, A.P. et al. (1995) In: *Neptune and Triton*, D.P. Cruikshank (ed.), University of Arizona Press, Tucson, pp. 613–682.
Ingersoll, A.P. and P.-G. Cuong (1981) *J. Atmos. Sci.*, **38**, pp. 2067–2076.
Ingersoll, A.P. and H. Kanamori (1995) *Nature*, **374**, pp. 706–708.
Ingersoll, A.P. and C.C. Porco (1978) *Icarus*, **35**, pp. 27–43.
Ingersoll, A.P. et al. (1997) *Icarus*, submitted.
MacLow, M.-M. and A.P. Ingersoll (1986) *Icarus*, **65**, pp. 353–369.
Niemann, H.B. et al. (1996) *Science*, **272**, pp. 846–849.
Niemann, H.B. et al. (1997) *J. Geophys. Res.*, in press.
Pollack, J.B. et al. (1992) *Space Sci. Rev.*, **60**, pp. 143–178.
Roos-Serote, M. et al. (1997) *J. Geophys. Res.*, submitted.
Showman, A.P. and A.P. Ingersoll (1997) *Icarus*, submitted.
Smith, B.A. et al. (1979a) *Science*, **204**, pp. 951–972.
Smith, B.A. et al. (1979b) *Science*, **206**, pp. 927–950.
Sromovsky, L.A. et al. (1996) *Science*, **272**, pp. 851–854.
Terrile, R.J. and R.F. Beebe (1979) *Science*, **204**, pp. 948–951.
Vasavada, A.R. et al. (1997) *Icarus*, submitted.